6770–6786 *Nucleic Acids Research, 2016, Vol. 44, No. 14* *Published online 12 May 2016*
doi: 10.1093/nar/gkw411

Dual daughter strand incision is processive and increases the efficiency of DNA mismatch repair

Nicolaas Hermans[1,†], Charlie Laffeber[1,†], Michele Cristovão[1], Mariela Artola-Borán[2], Yannicka Mardenborough[1], Pauline Ikpa[1], Aruna Jaddoe[1], Herrie H.K. Winterwerp[3], Claire Wyman[1,4], Josef Jiricny[2], Roland Kanaar[1,4], Peter Friedhoff[5] and Joyce H.G. Lebbink[1,4,*]

[1]Department of Molecular Genetics, Cancer Genomics Netherlands, Erasmus Medical Center Rotterdam, 3015 AA Rotterdam,The Netherlands, [2]Institute of Molecular Cancer Research of the University of Zurich and ETH Zurich, Winterthurerstrasse 190, CH 8057 Zurich, Switzerland, [3]Division of Biochemistry and Center for Biomedical Genetics, Netherlands Cancer Institute, 1006 BE Amsterdam, The Netherlands, [4]Department of Radiation Oncology, Erasmus Medical Center Rotterdam, 3015 CE Rotterdam, The Netherlands and [5]Institute for Biochemistry, Justus-Liebig-University, D-35392 Giessen, Germany

Received November 19, 2014; Revised April 29, 2016; Accepted May 03, 2016

ABSTRACT

DNA mismatch repair (MMR) is an evolutionarily-conserved process responsible for the repair of replication errors. In *Escherichia coli,* MMR is initiated by MutS and MutL, which activate MutH to incise transiently-hemimethylated GATC sites. MMR efficiency depends on the distribution of these GATC sites. To understand which molecular events determine repair efficiency, we quantitatively studied the effect of strand incision on unwinding and excision activity. The distance between mismatch and GATC site did not influence the strand incision rate, and an increase in the number of sites enhanced incision only to a minor extent. Two GATC sites were incised by the same activated MMR complex in a processive manner, with MutS, the closed form of MutL and MutH displaying different roles. Unwinding and strand excision were more efficient on a substrate with two nicks flanking the mismatch, as compared to substrates containing a single nick or two nicks on the same side of the mismatch. Introduction of multiple nicks by the human MutLα endonuclease also contributed to increased repair efficiency. Our data support a general model of prokaryotic and eukaryotic MMR in which, despite mechanistic differences, mismatch-activated complexes facilitate efficient repair by creating multiple daughter strand nicks.

INTRODUCTION

DNA mismatch repair (MMR) is crucial for the maintenance of genomic stability. Malfunction of MMR results in a 100 to 1000-fold increase in spontaneous mutation rates and is associated with Lynch syndrome in humans (1,2). MMR has many functions that involve the recognition of mispaired bases, most notably the strand-specific correction of mismatches and small insertion/deletion loops remaining after replication (1). The MMR pathway of *Escherichia coli* was the first to be reconstituted *in vitro* from purified components (3). The three proteins MutS, MutL and MutH are sufficient for mismatch recognition and endonucleolytic incision of the newly-synthesized DNA strand (4). Subsequently, DNA helicase II (UvrD) is loaded onto the DNA by MutL and unwinds the incised strand from the nick toward the mismatch in a 3′ to 5′ direction (5). The exonucleases RecJ, ExoI, ExoVII and ExoX then degrade the displaced strand containing the replication error, the resulting single-stranded gap is filled-in by repair synthesis and the remaining nick is sealed by a DNA ligase (6). In eukaryotes, several homologues of MutS and MutL are present (2). The two MutS homologues that play a role in MMR are MutSα (a heterodimer of MSH2 and MSH6) and MutSβ (a heterodimer of MSH2 and MSH3). The functional homologue of MutL is MutLα (a heterodimer of MLH1 and PMS2). Following recognition of the mismatch and the strand discrimination signal, daughter strand removal is accomplished either *via* Exonuclease I (7,8) or *via* strand displacement by DNA polymerase δ (9), after which resynthesis and ligation take place.

*To whom correspondence should be addressed. Tel: +31 10 7030473; Email: j.lebbink@erasmusmc.nl
†These authors contributed equally to the work as first authors.
Present address: Nicolaas Hermans, Biological and Soft Matter Physics, Huygens-Kamerlingh Onnes Laboratory, Leiden University, Leiden, The Netherlands.

E. coli MutS and human MutSα recognize base-base mismatches and small insertion and deletion loops (10–14). Mismatch binding by MutS or MutSα triggers an ATP-dependent conformational change into a ring-like structure that releases the mismatch and diffuses along the DNA contour (15–18). This so-called sliding clamp can recruit MutL or MutLα, respectively (16,19–22). Adenosine triphosphate (ATP) binding by *E.coli* MutL results in a conformational change that is required to activate the endonuclease MutH (23) and the UvrD helicase (24). Likewise, ATP is required to activate downstream steps in human MMR (25).

MMR in *E. coli* differentiates between the nascent and template DNA strands using the methylation status of GATC sites in newly-replicated DNA (26). Because Dam methylase lags behind the replication fork by about a minute, the nascent strand remains transiently unmethylated (27,28). This provides the mismatch-activated MutS–MutL complex with a short time window in which to license the cryptic endonuclease activity of MutH to incise the nascent strand 5′ from the unmethylated deoxyadenosine within the GATC site (29). UvrD helicase then unwinds the daughter strand from the MutH-generated nick toward the mismatch to make it available for nucleolytic degradation (5). Organisms other than Gram-negative bacteria do not rely on hemimethylation of GATC sites for strand discrimination and, correspondingly, lack MutH (30). Instead, they harbor a latent endonuclease activity within MutL/MutLα (25,31), which can be activated by the β-clamp in bacteria or PCNA in eukaryotes (32–35). In eukaryotes, targeting of the nuclease activity to the daughter strand is proposed to be dictated by the orientation of the PCNA/MutLα complex on the newly-replicated DNA (32,36). In addition, pre-existing strand discontinuities, such as Okazaki fragment termini or transient strand breaks introduced by the removal of misincorporated ribonucleotides after replication (37,38), may also help direct MMR to the nascent strand.

Previous *in vitro* and *in vivo* experiments have shown that the efficiency of *E. coli* MMR depends on the number of hemimethylated GATC sites, as well as on the distance between the mismatch and the nearest GATC site (24,39–42). Increasing the distance from 1 to 6 kb abolished strand-specific repair *in vivo* (40), while MMR reconstituted from purified components lost its efficiency over distances of 2 kb (43). This suggests that the distance between a GATC site and the mismatch, and/or the number of sites, influence either strand discrimination, or excision of the mismatched base from the DNA. To distinguish between these possibilities, we quantified the effect of GATC site number and distribution on the efficiency of MutH activation, strand displacement by UvrD and degradation by ExoI, respectively. To obtain mechanistic insights, we quantified in detail the dependence of strand incision on the individual components MutS, MutL and MutH. Furthermore, we extended our analysis to mammalian MMR by analyzing the contribution of the MutLα endonuclease to repair efficiency. Based on our results, we propose a universal model for MMR in which, despite significant differences in the molecular mechanisms of daughter strand discrimination and incision between *E. coli* and humans, the coordinated introduction of multiple daughter strand nicks increases the overall repair efficiency.

MATERIALS AND METHODS

Protein purification

MutS, MutL, MutH and UvrD were purified and stored as described (44–48). MutL N302A and K307A were derived from pTX418 (49) using QuikChange (Stratagene) and purified as wild type MutL. Protein concentrations were determined spectrophotometrically ($\epsilon^{280\,nm} = 73\,605\ M^{-1}\ cm^{-1}$ for MutS; $54\,270\ M^{-1}\ cm^{-1}$ for MutL; $38\,023\ M^{-1}\ cm^{-1}$ for MutH; $105\,000\ M^{-1}\ cm^{-1}$ for UvrD (50)). Wild type MutLα and the nuclease-deficient variant MLH1/PMS2-D699N were purified as described (21). ExoI and Ssb were purchased from New England Biolabs (Ipswich, USA) and Promega (Madison, USA), respectively.

DNA substrates

Templates for generation of hemimethylated DNA substrates were created from a derivative of pGEM13Zf (51) by removal of specific GATC sites using site-directed mutagenesis (Quikchange, Stratagene). Resulting template phagemids were GATC1 (3196 bp with one GATC site at position 2154), GATC2 (3198 bp with two GATC sites at position 2156 and position 31) and GATC15 (3195 bp, 15 GATC sites; sequences provided in the Supplementary Data). Hemimethylated DNA substrates (Supplementary Figure S1) containing a single G/T mismatch or corresponding A/T Watson–Crick base pair were constructed by extending a primer containing an Alexa Fluor ® 647 ($Alexa^{647}$) or Alexa Fluor ® 488 ($Alexa^{488}$) fluorophore (IBA GmbH, Göttingen, Germany) or no fluorophore on single-stranded (ss)DNA derived from phagemids GATC1, GATC2 or GATC15 as described (51), with the exception that closed circular DNA was gel-purified using a Promega gel purification kit. Primer GT14 (5′-CCAGACGTCTGTC-g-ACGTTGGGAAGCT-T*-GAGTATTCTATAGTGTCACCT-3′, where the g indicates the nucleotide forming the G/T mismatch, and the T* is the Alexa-labeled nucleotide) was used to create substrates GT#1 (G/T mismatch at position 1, with one GATC site 1042 bp 3’ of the mismatch), GT#2 (mismatch at position 1 and two GATC sites 1042 bp 3′ and 31 bp 5′ from the mismatch), GT#15 (mismatch at position 1 and 15 GATC sites, closest GATC site 14 bp 5′ from the mismatch). Homoduplex substrate was generated in the same way, using the primer AT14: (5′-CCAGACGTCTGTC-a-ACGTTGGGAAGCT-T*-GAGTATTCTATAGTGTCACCT-3′). GT28 (5′-GGTAGCTCTTCA-T*-CCGGCAAACAAACC-g-CCGCTGGTAGCG-3′) was used to create GT#1b (GT mismatch at position 2215, one GATC site which is 61 bp 3′ from the mismatch); GT#2b (mismatch at position 2217 and two GATC sites, one which is 61 bp 3′ from the mismatch and one which is 1012 bp 5′ from the mismatch; GT#15b (G/T mismatch at position 2214, 14 GATC sites (1 removed due to primer inadvertently introducing a C/C mismatch at position 2221 on top of existing GATC site in original GATC15), closest GATC site 61 bp 3′ from the G/T mismatch).

In unwinding and excision experiments using pre-nicked substrates, GT#1b was pre-nicked with Cas9-D10A nick-

ase preloaded with the appropriate tracrRNa and crRNA. Cas9-D10A was purchased from PNABIO (Thousand Oaks, USA). TracrRNA and crRNA were purchased from IDT (Leuven, Belgium) with the variable sequence of the crRNAs being 5′-CUUCUAGUGUAGCCGUAGUU (CrA) for creation of a nick at position 2314 on GT#1b (160 bp 5′ from GATC, 99 bp 5′ from mismatch) and 5′-UUUUUAAUUUAAAAGGAUGU (CrB) for the creation of a nick at position 2046 on GT#1b (169 bp 3′ from the mismatch and 108 bp 3′ from the GATC). TracrRNA–crRNA duplex was formed by incubating a mixture containing 3 μM of each oligonucleotide in IDT duplex buffer (IDT, Leuven, Belgium) at 95°C for 5 min, and slow cooling at room temperature. The pre-nicking reaction contained 5 μg (0.5 pmol) of DNA substrate GT#1b, 5 μg (30 pmol) Cas9-D10A and 90 pmol of duplex tracr-crRNA in a total reaction volume of 200 μl in 1x NEB 3.1 buffer (New England Biolabs). The reaction was incubated for one hour at 37°C and stopped at 70°C for 20 min. The nicked substrate was purified from 1% agarose gel run in TAE buffer supplemented with 0.5 μg/ml ethidium bromide (EtBr), using the Promega Wizard SV Gel & PCR Cleanup Kit (Promega, Madison, USA).

Substrates for mismatch repair in human nuclear extracts were generated as described previously (51). Briefly, the heteroduplexes containing a G/T mismatch within an AclI restriction site in the 46-bp polylinker of a pGEM13Zf(+) derivative were constructed by primer extension, using the mismatch-containing oligonucleotide (G/T: 5′-AGA CGT CTG TC**G** ACG TTG GGA AGC TTG AG-3′) as primer (the mispaired residue is highlighted in bold) and the single-stranded phagemid DNA carrying one Nt.BstNBI nicking site 363 bp 5′ from the mismatch, one Nb.BtsI nicking site 184 bp 3′ from the mismatch or both as template. After primer extension, ligation and isolation of the desired supercoiled heteroduplex substrates on CsCl gradients, substrates were nicked with Nt.BstNBI and Nb.BtsI (New England Biolabs) as indicated by the manufacturer. The products were then loaded on a 1% agarose gel and visualized with GelRed.

Size exclusion chromatography

MutL (1.5 mg/ml) in 25 mM Hepes-KOH pH 7.5, 150 mM KCl, 5 mM $MgCl_2$, 10% glycerol, 10 mM β-mercaptoethanol was mixed with 1 mM adenosine diphosphate (ADP), ATP or adenylylimidodiphosphate (AMPPNP), or buffer as control, incubated for 16 h at 4°C and injected on an Superdex 200 size exclusion column equilibrated in 25 mM Hepes-KOH pH 7.5, 150 mM KCl, 5 mM $MgCl_2$, 10% glycerol and operated by an ÄktaMikro (GE Healthcare). Elution was monitored at 260 and 280 nm wavelengths.

MutH activation assay

Standard incision assays were performed with 10 nM MutS, 10 nM MutL, 5 nM MutH and 0.5 nM Alexa^{647}-labeled circular relaxed DNA substrate at 37°C in standard assay buffer (25 mM Hepes KOH [pH 7.5], 150 mM KCl, 5 mM $MgCl_2$, 10% glycerol, 100 ng/μl BSA, 1 mM DTT, 0.005% Tween 20) containing 1 mM ATP. Variations of these conditions included 50 instead of 150 mM KCl to be able to observe nicking in the absence of MutS, increased concentration of DNA (5 nM) and varying concentrations of MutS, MutL and MutH (between 0 and 500 nM as indicated). Unless stated otherwise, reactions were started by adding a mix of ATP and DNA to a mixture of MutS, MutL and MutH. The reactions (10 μl) were stopped with an equal volume of 20% glycerol, 1% SDS and 50 mM EDTA and analyzed on 0.8% agarose gels run in TAE buffer in the presence of 0.5 μg/ml ethidium bromide to distinguish covalently-closed double-stranded (ds)DNA substrate from nicked circular dsDNA product. To denature dsDNA circles into ssDNA fragments, reactions (10 μl) were stopped at indicated time points by adding 15 μl buffer containing 8 M Urea and 1% SDS. Samples were denatured by incubation for 10 min at 85°C and run on a 1.5% agarose gel in TAE buffer and 1 M urea, as described (52).

To address distance dependence at protein concentrations approaching saturation (200 nM MutS, 200 nM MutL, 50 nM MutH), we mixed 2 nM DNA substrates containing a single GATC site located either 32 bp or 1041 bp from the mismatch and different fluorophores to accurately determine nicking efficiencies within one experiment of 20 s duration. Reactions were stopped by adding an equal volume of 20% glycerol, 1% SDS, 50 mM EDTA and run on a 1% agarose gel containing 40 μM chloroquine to supercoil closed circular substrate and allow monitoring of the signal of both the Alexa^{488} and Alexa^{647} fluorophores.

Unwinding and excision assays

Nicking and subsequent unwinding and excision was monitored by supplementing standard nicking reactions (10 nM MutS, 10 nM MutL, 5 nM MutH) with 5 nM UvrD, 200 nM Ssb, 0.1 units of ExoI and 1 mM ATP, using substrates GT#1, GT#1b, GT#2, GT#2b, GT#15 and GT#15b. Reaction mixtures were analyzed on 1% agarose gels by quantifying the amount of fluorescent signal from Alexa^{647}-labeled substrate and nicked circular DNA. Unwinding and excision on pre-nicked substrates was performed at identical conditions using GT#1b pre-nicked with 10 nM MutS, 10 nM MutL and 5 nM MutH, with MutSLH and Cas9-D10A-CrA or with MutSLH and Cas9-D10A-CrB. Controls were incubated 10 min at 70°C to inactive MutSLH before addition of UvrD, Ssb and ExoI.

Mismatch repair in human nuclear extracts

MMR reactions in MutLα-deficient human extracts, supplemented with wild type or nuclease-deficient MutLα D699N as indicated, were carried out as described (51) on substrates carrying nicks either 3′ or 5′ from the mismatch or both. MMR reactions contained 275 ng of each DNA substrate and 275 μg of HEK293T nuclear extracts supplemented where indicated with 0.7 pmol of wild type MutLα or the MutLα D699N mutant in a total volume of 70 μl in a buffer containing 20 mM Tris-HCl (pH 7.6), 5 mM $MgCl_2$, 110 mM KCl, 1 mM glutathione, 50 μg/ml BSA, 100 μM dNTPs. The extracts were incubated at 37°C and 12.5 μl aliquots were withdrawn at the indicated time points. The

reaction was stopped by adding an equal volume of 2x stop solution containing 1 mM EDTA, 3% SDS and 5 mg/ml proteinase K. The samples were incubated at 55°C for 3 h, purified on Mini-Elute clean-up columns (Qiagen) and subjected to restriction digestion with AclI. The digested DNA was resolved on 1% agarose gels.

Quantification

Fractions of substrate, intermediate and products of incision and unwinding reactions were quantified by scanning the fluorescence of the Alexa-labeled DNA fragments separated by gel electrophoresis using a Typhoon9100 imager (GE Healthcare). The Alexa^{488} labeled DNA was excited with a 488 nm laser, and the Alexa^{647} labeled DNA was excited at 633 nm. Emission was passed through 520BP40 and 670BP30 filters, respectively. Band intensities were quantified using NIH ImageJ (Rasband, W.S., ImageJ, U.S. National Institutes of Health, Bethesda, Maryland, USA, http://imagej.nih.gov/ij/, 1997–2012). Fractions of intact substrate, nicked intermediate and product were calculated relative to the total signal obtained from the fluorophore. In the case of control reactions using unlabeled DNA, the EtBr signal was quantified using the 532 excitation laser and filter 610BP30, taking into account that covalently closed and nicked circles stain differently and relative ratios of these forms cannot quantitatively be determined.

Fitting incision data from denaturing gels with the incision model

The incision model describes the exponential decay of the closed circular substrate (S) into single-nicked intermediate (I) and the subsequent exponential decay of this intermediate into double-nicked product (P) as a function of time t. This model was fit to the fractions of substrate, intermediate and product obtained from the incision experiments using a global fit of the following equations in Graphpad Prism (version 5):

$$S\ (t) = S_0\ e^{-k_1 t}$$

$$I\ (t) = [(k_1 S_0) / (k_2 - k_1)]\ * \left[e^{-k_1 t} - e^{-k_2 t}\right]$$

$$P\ (t) = S_0\ * \left[1 - \left\{\frac{1}{k_2 - k_1}\right\} * \left\{k_2 e^{-k_1 t} - k_1 e^{-k_2 t}\right\}\right]$$

where S_0 is the fraction of closed circular substrate at time 0 and k_1 and k_2 are the rate constants for the first and the second incision, respectively.

Fitting data with the unwinding model

The unwinding model describes the exponential decay of unnicked circular substrate (S) into nicked intermediate (I) and the subsequent exponential decay of this intermediate into unwound and degraded product. This model was fit to the fractions of substrate, intermediate and product obtained from the unwinding experiments using a global fit in Graphpad Prism:

$$S\ (t) = S_0\ e^{-k_1 t}$$

$$I\ (t) = [(k_1 S_0) / (k_3 - k_1)]\ * \left[e^{-k_1 t} - e^{-k_3 t}\right] + C$$

where S_0 is the fraction of closed circular substrate at time 0, t is the time, C is the plateau value reached for I and k_1 and k_3 are the rate constants for incision and unwinding/excision, respectively.

RESULTS

Effect of GATC site distribution on the efficiency of daughter strand incision

To investigate at which step of the mismatch repair reaction the GATC site distribution exerts its effect (39–41), we developed a mismatch-specific, quantitative incision assay using circular DNA substrates carrying a single G/T mismatch or the corresponding A/T Watson–Crick base pair, either 1, 2 or 15 hemimethylated GATC sites and an Alexa^{647} or Alexa^{488} fluorophore (elaborate controls in Supplementary Data, Supplementary Figures S1 and S2). We found that the action of MutH as a MutSL-independent nuclease at 50 mM KCl depends on the number of GATC sites (Figure 1A), indicating that under these conditions the search for the GATC site was rate limiting for incision. At physiological salt conditions, mismatch-dependent MutSLH-induced incision was almost completely independent of the number of GATC sites (Figure 1B) and comparable to rates reported in literature on circular substrates (0.05 mol DNA/mol MutS/min for 20 nM MutS, 10 nM MutL, 5 nM MutH in our assay, compared to 0.007 mol DNA/mol MutS/min for 35 nM MutS, 24 nM MutL, 1 nM MutH (53)). Furthermore, at high protein concentration approaching saturation (Supplementary Figure S1F), thereby maximizing the rate of protein complex formation and mimicking the *in vivo* situation (54), incision efficiency was independent of the distance between the mismatch and the GATC site (Figure 1C and D). Under these conditions we observed a lag phase before the initiation of incision (Figure 1D), indicating that a reaction step before finding the GATC site becomes rate-limiting for incision.

Multiple hemimethylated GATC sites were nicked in rapid succession

To monitor two separate nicking events on the same DNA molecule, incision of the substrate containing two GATC sites (GT#2) was resolved using gel electrophoresis under denaturing conditions (Figure 2). At 50 mM KCl, MutH acted as a MutS- and MutL-independent endonuclease (Figure 2A). At 150 mM KCl, 250 nM MutH could not efficiently incise GT#2 (Figure 2B). Considering the MutH incision activity at 50 mM KCl as a distributive process with both nicking events being independent, we could model the formation of the intermediate with a single nick as an exponential decay of the closed circular DNA, and formation of the product with two nicks as an exponential decay of the intermediate with one nick (Figure 2E). This incision model fitted the activity of 250 nM MutH at 50 mM KCl on 0.5 nM GT#2 (Figure 2F), with an observed rate for the first incision of 0.31 ± 0.005 nM GT#2/min and the second incision of 0.11 ± 0.002 nM GT#2/min (Supplementary Table S1). The slower rate of the second nicking event

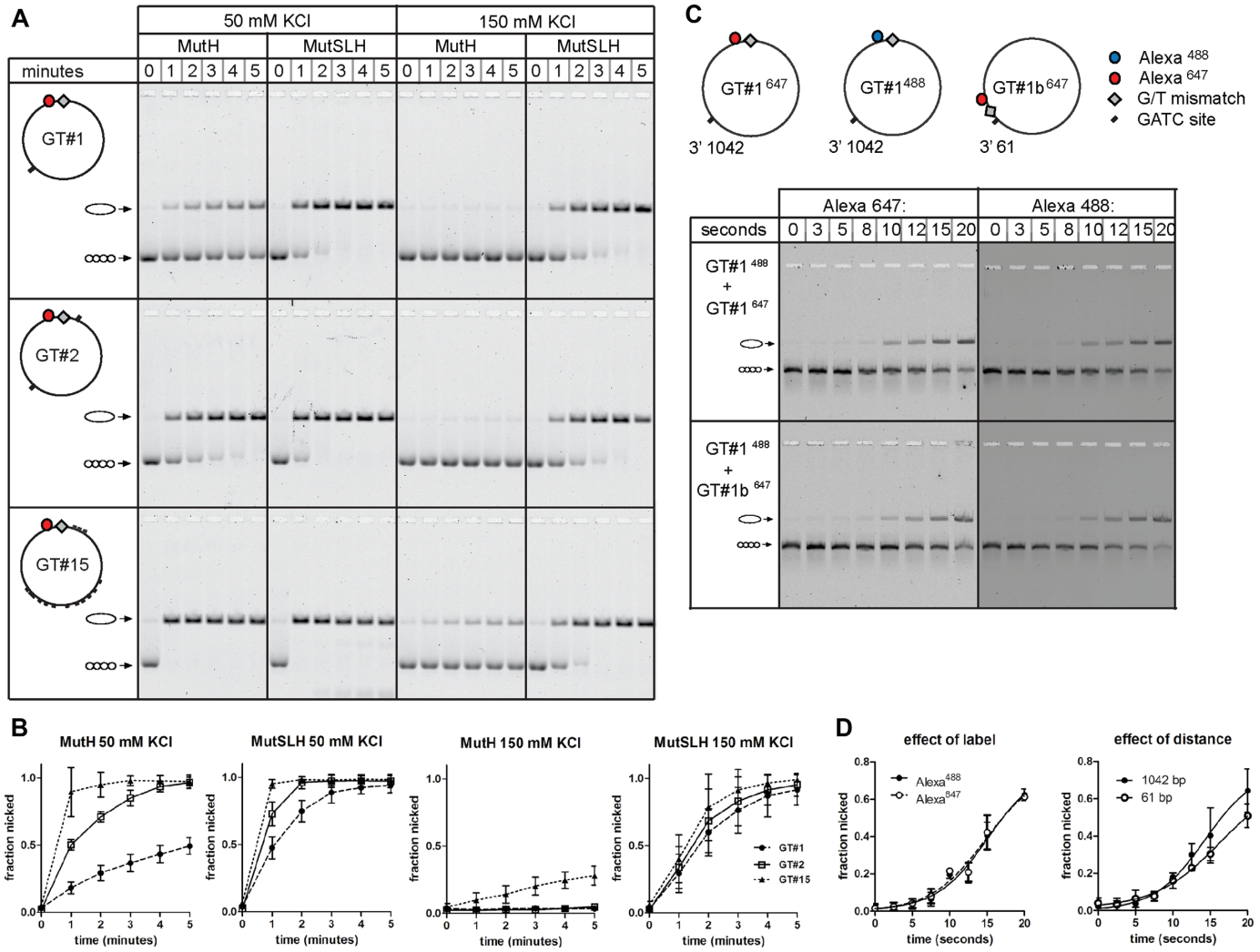

Figure 1. Influence of GATC site distribution (number and location) on the efficiency of daughter strand incision. (**A**) Time courses of incision of 0.5 nM GT#1, GT#2 and GT#15 substrates by 250 nM MutH or 10 nM MutS, 10 nM MutL, 250 nM MutH at 50 and 150 mM KCl. Substrates carried a single G/T mismatch, a fluorescent label for quantification and 1, 2 or 15 hemi-methylated GATC sites as indicated. Reaction products were separated by agarose gel electrophoresis in the presence of EtBr to separate the covalently-closed substrate from the nicked product. (**B**) Quantification of the fraction of the nicked product (mean ± SD, n = 3). (**C**) Time courses showing the Alexa^{647} and Alexa^{488} signals of mixtures of differentially-labeled mismatched substrates with different distances between the mismatch and the single GATC site, nicked by 200 nM MutS, 200 nM MutL, 50 nM MutH. Upper panels: incision time course of a mixture of 1 nM GT#1^{488} and 1 nM GT#1^{647}, to verify that the fluorescent labels did not affect incision rates. Lower panels: incision time course of a mixture of 1 nM GT#1^{488} and 1 nM GT#1b^{647}, to compare within the same experiment the rate of incision of the same GATC site when a G/T mismatch was located either 1041 (in GT#1) or 60 bp away (in GT#1b). (**D**) Quantitation of time courses (mean ± SD, n = 3).

reflects the reduction in effective GATC site concentration after nicking of the first site (MutH may resample the incised GATC site), and/or a sequence context effect. Fitting the incision model to the data obtained with 250 nM MutH at 50 mM KCl on 5 nM DNA (Supplementary Figure S3A and B, left panels) returned observed rates of 3.8 ± 0.2 and 1.0 ± 0.06 nM DNA/min for the first and second incision, respectively. These rates were approximately ten times faster than on 0.5 nM DNA and are in full agreement with recognition of the GATC site by MutH being rate-limiting under these conditions. The addition of MutL did not affect nicking rates at 50 mM KCl, and did not enable incision at 150 mM KCl (Supplementary Figure S4; Table S1).

We resolved mismatch-dependent incision by MutH by adding 10 nM MutS and 10 nM MutL. At 50 mM KCl (Figure 2C), both MutH and MutSLH-dependent nicking events are expected to occur, and the observed rates for the first incision (0.44 ± 0.02 nM GT#2/min) and especially the second incision (0.47 ± 0.03 nM GT#2/min) were increased compared to the rates obtained with MutH alone (Supplementary Table S1). At 150 mM KCl (Figure 2D), at which all incision events are mismatch-dependent (see Supplementary Figure S4 for homoduplex controls), the single-nicked intermediate was barely detectable, indicating that the substrate was rapidly converted into a product on which both GATC sites were nicked. This was reflected in the observed rates obtained from fitting the incision model to the data, with the second incision (1.1 ± 0.1 nM DNA/min) now being significantly faster than the first (0.28 ± 0.01 nM DNA/min) (Supplementary Table S1).

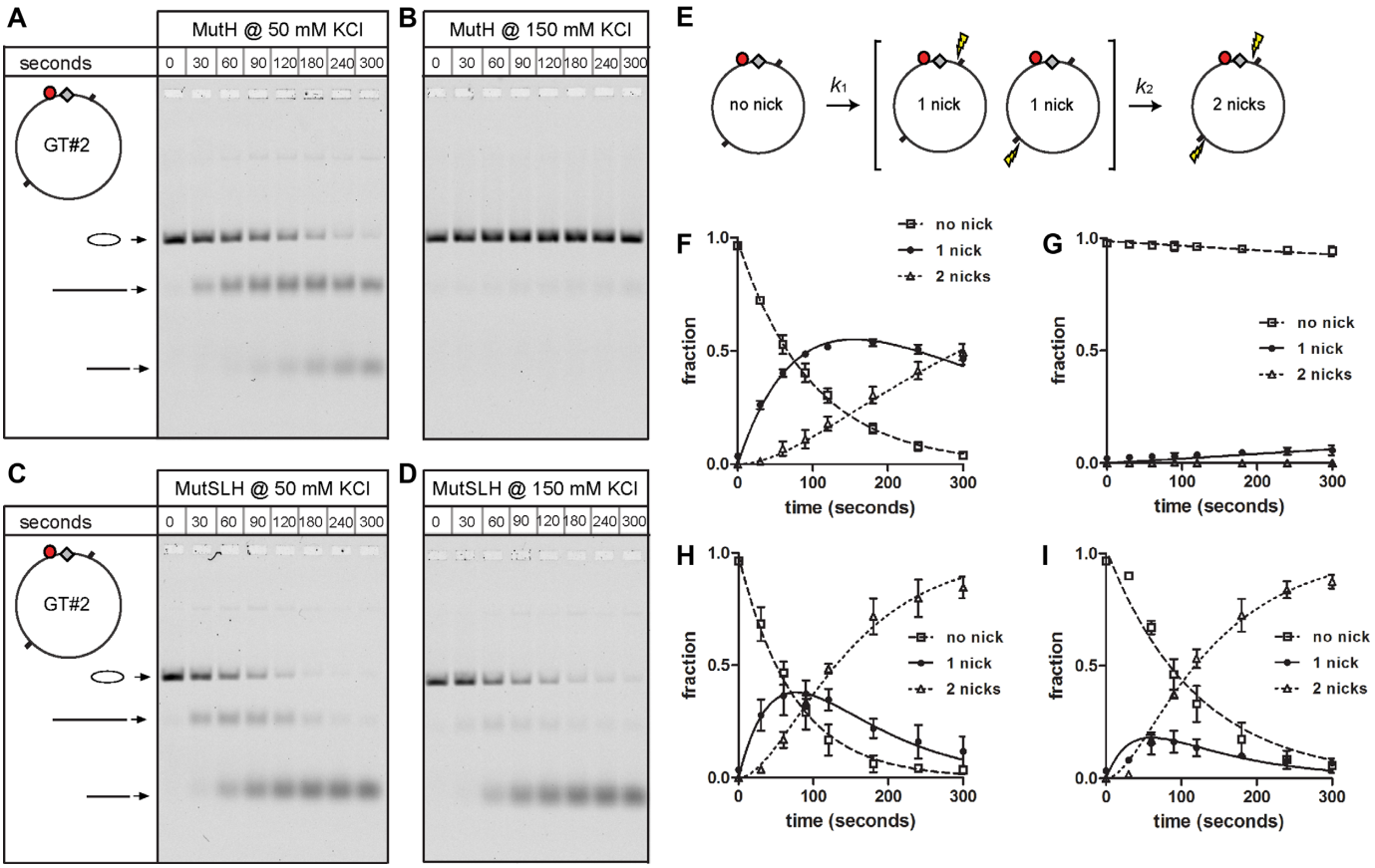

Figure 2. MutS and MutL modulate dual GATC site incision by MutH. (**A**) Denaturing agarose gel separating the labeled ssDNA fragments obtained from 0.5 nM GT#2 nicked by 250 nM MutH in low salt (50 mM KCl), with upper band representing the covalently-closed substrate, the middle band the intermediate with a single nick and the lower band the product resulting from two nicking events. (**B**) At 150 mM KCl, 250 nM MutH incised 0.5 nM GT#2 with very low efficiency. (**C**) At 50 mM KCl, the addition of 10 nM MutS and 10 nM MutL increased incision of GT#2 by 250 nM MutH. (**D**) At 150 mM KCl, the pattern of GT#2 incision products formed by 10 nM MutS, 10 nM MutL and 250 nM MutH differed from that at 50 mM KCl. (**E**) Model representation of the incision reaction on GT#2 with kinetic constants k_1 and k_2 describing the conversion of the covalently-closed substrate into single-nicked intermediate and conversion of this intermediate into double-nicked product, respectively. (**F**–**I**) Quantification of the fraction of GT#2 containing no nick (□), one nick (●) and two nicks (Δ) from experiments as shown in panels A–D, respectively (mean ± SD, n ≥ 2) with fit of the incision model (lines). Rate constants obtained from the fits are tabulated in Supplementary Table S1.

The two incisions were thus not independent, consecutive events. Either the incision events occurred almost concurrently, with the second event initiating before completion of the first event; or the incision of the second site was faster than that of the first, made possible by the sharing of a rate-limiting step such as the assembly of a pre-incision complex. Moreover, incision of multiple sites on GT#15 (carrying 15 GATC sites) occurred to apparent completion within the same timeframe as on GT#2 (Supplementary Figure S5), indicating that rapid multiple incision was not restricted to two GATC sites. Whether the multiple incisions are introduced in a processive manner, or whether multiple loading can fully account for the observed effect is further considered below.

A single mismatch-activated MMR complex enabled dual incision in a processive manner

To reduce multiple loading of MutS, we increased the concentration of the DNA substrate from 0.5 to 5 nM (Figure 3A) such that the effective concentration of MutS and MutL dimers was equimolar to the concentration of mismatched DNA molecules. At 150 mM KCl (Figure 3A), the rate of the first incision doubled (from 0.28 ± 0.01 to 0.60 ± 0.02 nM DNA/min), due to faster binding of MutS to DNA (Figure 3B, Supplementary Table S1). The appearance of the second nick still occurred rapidly after the first, since accumulation of the intermediate with a single nick was even lower than at 0.5 nM DNA concentration (Figure 3A and B), and the second incision again occurred approximately four times faster than the first (2.2 ± 0.2 nM DNA/min, Supplementary Table S1). Similarly, reducing the frequency of multiple loading events by lowering MutS and MutL concentrations to 2 nM rather than increasing the number of DNA molecules resulted in a 6-fold faster rate for the second incision compared to the first (Supplementary Table S1). Reducing the frequency of multiple loading events thus did not abolish rapid dual incision.

To further address processive incision activity in the absence of multiple loading of MutS, we created single turnover conditions in which only the first MutS bound to the mismatch was able to proceed and activate MutH. In

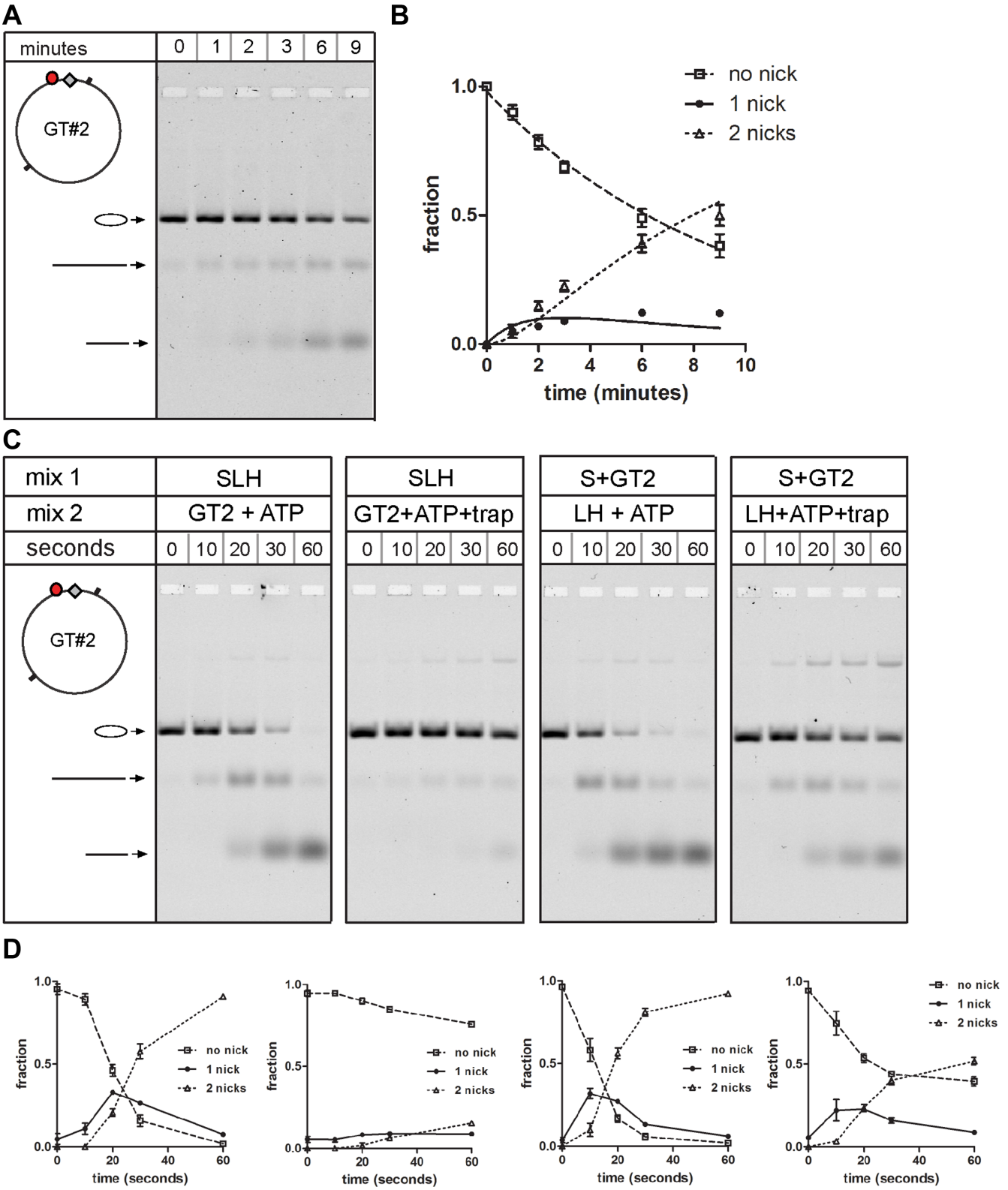

Figure 3. Processive dual GATC site incision by MutSLH at 150 mM KCl. (**A**) Near absence of single-nicked intermediate upon incision of 5 nM GT#2 by 10 nM MutS, 10 nM MutL and 250 nM MutH. (**B**) Quantification of the incision of 5 nM GT#2 by 10 nM MutS, 10 nM MutL, 250 nM MutH and fit with the incision model. Rate constants obtained from the fit are tabulated in Supplementary Table S1. (**C**) Processive incision of GT#2 under single turnover conditions. Panel 1: 50 nM MutS, 50 nM MutL, 25 nM MutH is mixed with 0.5 nM GT#2 and ATP (standard reaction). Panel 2: MutSLH was mixed with GT#2, ATP and 25 nM unlabeled GT#2 which acts as a trap by binding MutS and preventing incision of the labeled DNA. Panel 3: 50 nM MutS was prebound to 0.5 nM GT#2 and the reaction was started by addition of MutLH and ATP. Panel 4: 50 nM MutS was prebound to 0.5 nM GT#2 and mixed with MutLH, ATP and 25 nM unlabeled GT#2 (trap DNA). Under these conditions only prebound MutS that was able to switch into the activated clamp state could proceed with incision of the labeled GT#2. (**D**) Quantifications of the single-turnover reactions.

this experiment, addition of excess unlabeled GT#2 (trap DNA) to the labeled DNA prior to starting the reaction was able to almost completely inhibit incision (Figure 3C compare panel 1 and 2). We predicted that addition of the DNA trap after preassembly of MutS-mismatched DNA complexes would inhibit additional loading after the first MutS releases the mismatch. Under these conditions, approximately 60% of the DNA was processed (Figure 3C panel 4), reflecting the fraction of mismatch-bound MutS able to be activated toward sliding clamp upon initiation of the reaction (55). Notably, the majority (86%) of this fraction was rapidly converted into the product containing two nicks. We therefore conclude that a single mismatch-activated MMR incision complex enables dual GATC site incision in a processive manner.

Dependence of processivity on MutSLH concentrations

We investigated the dependence of incision rates on the concentration of the single protein components, while keeping concentrations of the other two proteins and DNA constant and stoichiometric to minimize multiple loading (10 nM MutS and MutL which equals 5 nM dimer each; 5 nM MutH and 5 nM DNA). The rate of the first incision varied with the concentration of all three proteins, but was most sensitive to the concentration of MutS (Figure 4A). The rate of the second incision was independent of the MutS concentration (Figure 4B), which is another indication that MutS does not have to be reloaded for the second incision and the first MutS acts in a processive manner. In contrast, the second incision did depend on the concentrations of MutH and especially MutL (Figure 4B), suggesting that both these proteins are reloaded for the second incision and are not an integral part of the processive MMR complex. Further increasing MutL and MutH concentrations indicated that above 10 nM, MutH becomes saturating, while both the first and second incision rate continued to rise with the MutL concentration (Supplementary Table S1). The difference in behavior between MutS on the one hand and MutL and MutH on the other hand is reflected in the ratio k_2/k_1 (Figure 4C).

To investigate the behavior of the system at conditions allowing multiple loading we kept the DNA concentrations low (0.5 nM) and varied protein concentrations. The rate of the first incision was again mostly determined by MutS; increasing MutL, MutH or both with MutS constant at 10 nM did not change k_1 more than 2-fold, while it changed 5-fold upon varying MutS (Figure 4D, 4 panels on the left; Supplementary Table S1). Unlike conditions with stoichiometric MutS and DNA concentrations, MutS in excess of DNA also influences k_2, to the same extent as MutL and MutH (Supplementary Table S1), indicating that multiple loading indeed occurred and increased the apparent incision rate of the second GATC site. Raising MutS to 100 nM had a large effect on the first incision (increase from 0.30 to 1.3 nM DNA/min), and a smaller effect on the second incision (from 0.89 to 1.5 nM DNA/min), but changing MutL or MutH independently did not have an effect (Supplementary Table S1). Increasing both MutL and MutH when MutS was at 100 nM enhanced the rate of the second incision (Supplementary Table S1). Further elevating MutS to 500 nM revealed an interesting effect; at high concentrations of MutL the system was fully active, however, at substoichiometric MutL concentrations, the first incision was still rapid but the second incision was largely inhibited, independent of the MutH concentration (Figure 4D, right panels, Supplementary Table S1). Thus, at specific conditions of high MutS concentrations enabling multiple loading, and limiting MutL concentrations, incision is still possible, but no longer processive. This again is an indication for a new MutL being loaded for each incision.

The closed conformation of MutL is required for processive incision

To better understand the MutL-dependence of the reaction, we analyzed two MutL variants that are able to activate MutH but that have an impaired ATPase (23,56). MutL N302A still binds ATP but its rate of ATP hydrolysis is reduced, while MutL K307A has a reduced ATP binding capacity (56). Size-exclusion chromatography allowed separation of the nucleotide-free, open form of MutL from the more compact nucleotide-bound, closed form of MutL (45) (Figure 5A). While wild type MutL was solely observed in the closed conformation with a non-hydrolyzable analog of ATP (AMP.PNP; Figure 5A left panel), MutL N302A was also observed in the closed state with ATP and ADP, reflecting its inability to distinguish between nucleotide diphosphate and triphosphate (Figure 5A middle panel). MutL K307A was only observed in the open state (Figure 5A, right panel) and based on the ratio OD^{280nm}/OD^{260nm}, nucleotide binding could not be observed. MutL N302A was still able to efficiently activate MutH, with k_1 and k_2 both being 2-fold reduced compared to wild type MutL, indicating that incision was still processive (Figure 5B and C, first and second panel). However, MutL K307A was very inefficient at activating MutH and the reaction was no longer processive, k_2 being 7 times smaller rather than 2 times larger than k_1 (Supplementary Figure S6, left panel; Figure 5B and C third and fourth panels; Supplementary Table S1). For MutL K307A, increasing the MutH concentration from 50 to 250 nM resulted in a significant increase in incision efficiency, especially in k_2 (Figure 5B and C fourth panels; Supplementary Table S1; Supplementary Figure S6B and C for controls). Taken together, these results suggest that the nucleotide-bound, closed conformation of MutL is required to activate MutH at a GATC site and that MutH can partially restore the function of MutL K307A.

Nicks flanking the mismatch increase the rate of unwinding by UvrD

To address whether multiple nicks influence unwinding and excision of the nascent DNA strand, we added UvrD, Ssb and ExoI to the nicking reaction containing MutS, MutL, MutH and substrates with different GATC site configurations (Figure 6). The unwinding and excision can be monitored *via* decrease of fluorescence from the nicked circular DNA upon removal of the $Alexa^{647}$ fluorophore, which is located 14 bp 3′ from the G/T mismatch on GT#1 and which does not form a roadblock for unwinding and excision (Supplementary Figure S7). During the first 6 min of

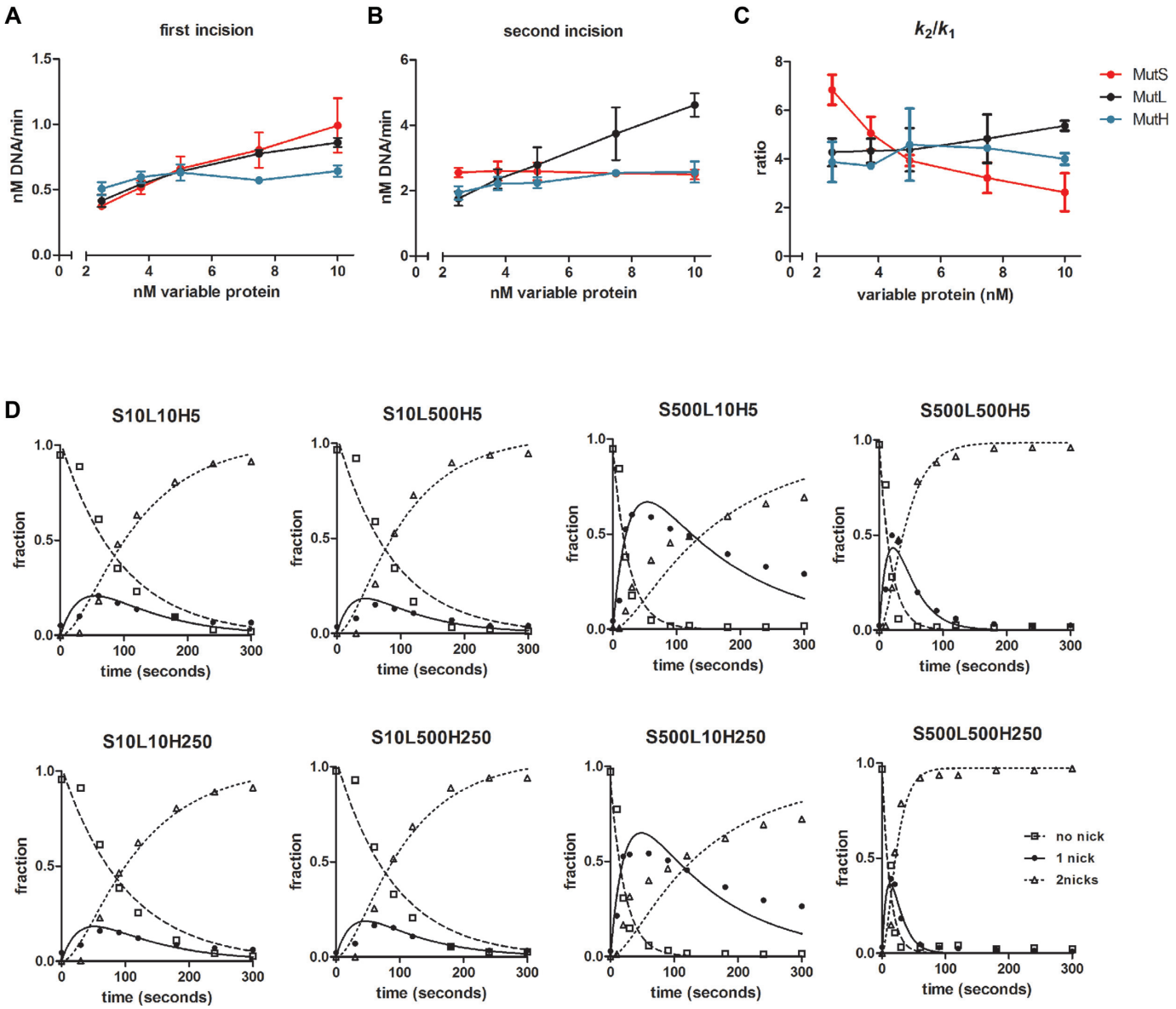

Figure 4. Titrations of MutS, MutL and MutH differentially influence rates of the first and second incisions. (**A**) Rates for incision (Supplementary Table S2) of the first GATC site on 5 nM GT#2 at varying concentrations of one protein (on the x-axis) and fixed concentrations (5 nM) of the other two. MutS and MutL are reported as dimers, MutH as a monomer. (**B**) Rates for incision (Supplementary Table S2) of the second GATC site on 5 nM GT#2 at varying concentrations of one protein and fixed concentrations (5 nM) of the other two. MutS and MutL are reported as dimers, MutH as monomer. (**C**) Ratio of k_2/k_1 for different variable protein concentrations. (**D**) Fractions of unnicked substrate, nicked intermediate and double-nicked product for titrations of high concentrations of MutS, MutL and MutH on 0.5 nM GT#2 and fit with the incision model (note that conditions in panel S10L10H250 are the same as in Figure 2I). Rate constants obtained from the fits are listed in Supplementary Table S1.

the reaction, all closed circular DNA substrates were nicked (Figure 6A), similar to nicking reactions without UvrD, Ssb and ExoI. Subsequently, the signal of the fluorophore disappeared over time, indicative of degradation of the region around the mismatch. This was dependent on the presence of UvrD and, to a lesser extent, on the presence of ExoI; when UvrD was absent, the DNA was not unwound or degraded (Supplementary Figure S8), and when ExoI was absent, the DNA was unwound but not degraded (Supplementary Figure S9, compare left and right panels).

First we analyzed the unwinding from a single GATC site, while varying the distance to the G/T mismatch. When the GATC site was located 1042 bp from the mismatch and the fluorophore (GT#1; Figure 6A first panel), a smear that migrated faster than the nicked DNA was observed, which most likely represented partially-degraded substrate in which the fluorophore was still present, formed by ExoI degrading the unwound strand from the 3′-end toward the mismatch. When the GATC site was located 61 bp from the mismatch and the fluorophore (GT#1b; Figure 6A second panel), no intermediate degradation products were detectable. We found a 3-fold difference in unwinding efficiency between these two substrates (quantified in Figure 6B first two panels; unwinding rate for GT#1 0.027 ± 0.003 nM

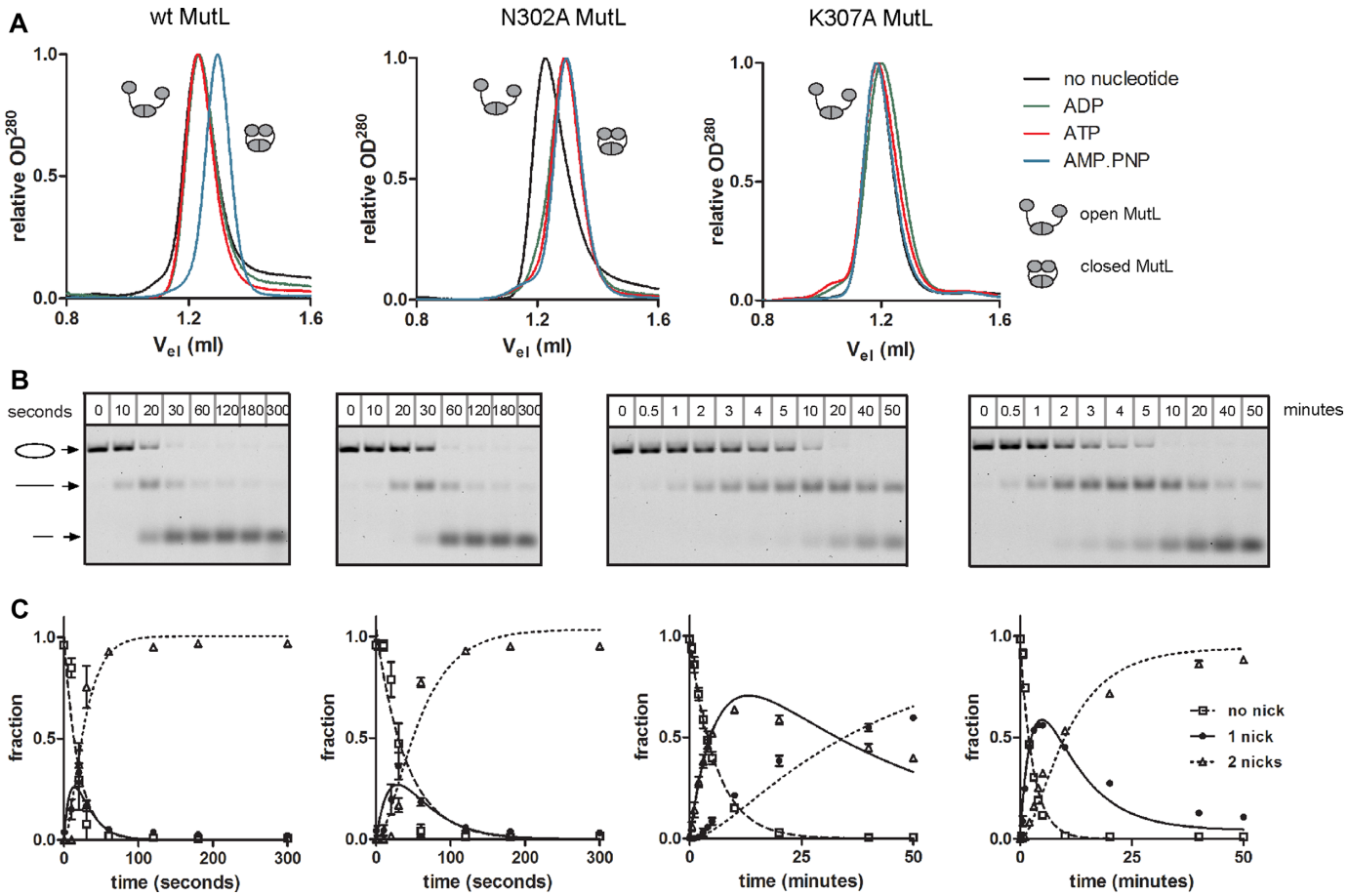

Figure 5. Processive strand incision requires the closed form of MutL. (**A**) Size exclusion chromatography of open and closed forms of MutL. Left panel: wild type MutL was observed in the open state without nucleotide (black), with ADP (green) and ATP (red), but closed with AMP.PNP (blue). MutL N302A was always observed in the closed state in the presence of nucleotide (middle panel) and MutL K307A was always observed in the open in the presence of nucleotides (right panel). (**B**) Incision of 0.5 nM GT#2 by 100 nM MutS, 100 nM MutL, 50 nM MutH with wild type (first panel), N302A (second panel) and K307A MutL variants (third panel with 50 nM MutH, fourth panel with 250 nM MutH). (**C**) Quantification (mean ± SD, n = 3) and fitting of strand incision by wild type, N302A and K307A MutL (with 50 and 250 nM MutH). Rate constants obtained from the fits are tabulated in Supplementary Table S1.

DNA/min and for GT#1b 0.075 ± 0.007 nM DNA/min, Supplementary Table S2), indicating that a misincorporated base close to the GATC site is excised faster than one located further away. We then tested the effect of a second GATC site 5′ from the mismatch (GT#2 and GT#2b), which provides an additional entry site for UvrD [the helicase can load both on the nicked and the intact strand and travel toward the mismatch in the 3′ to 5′ direction both from a 5′ and a 3′ nick] but not for ExoI (which is a 3′ to 5′ exonuclease (5,57)). Even with two GATC sites, the mismatch and the fluorophore can only be removed along the short path [which is preferred 10-fold over the long path; (5)] from a 3′ nick, which is the site 1042 bp from the mismatch (see cartoon above the gels in Figure 6A). Nevertheless, the excision rate further increased (0.084 ± 0.01 nM GT#2/min; 0.13 ± 0.009 nM GT#2b/min; Figure 6B panel 3 and 4; Supplementary Table S2). In contrast, additional GATC sites 3′ from the mismatch did not further increase the rates (0.10 ± 0.01 nM GT#15/min; 0.14 ± 0.02 nM GT#15b/min; Supplementary Table S2).

To establish to what extent the efficiency of unwinding and excision is influenced by the number of sites, by the distance of the sites from the mismatch, by the relative location of the sites with respect to the mismatch or a combination of these, we constructed three pre-nicked substrates with a single nick 61 bp 3′ from the mismatch, with two nicks located at 61 and 169 bp 3′ from the mismatch, and with two nicks flanking the mismatch at 61 bp 3′ and 102 bp 5′. We used two different CRISPR-RNAs to target Cas9-D10A to introduce additional nicks into MutSLH treated GT#1b (Figure 6C and D). Unwinding and excision rates were significantly faster on the substrate with two nicks, but especially and prominently when these were flanking the mismatch (0.051 ± 0.009 nM GT#1b/min; 0.087 ± 0.009 nM GT#1b-CrA/min; 1.1 ± 0.07 nM GT#1b-CrB/min; Supplementary Table S2). No unwinding and excision was observed upon heat inactivation of MutSLH prior to addition of UvrD, Ssb and ExoI, indicating that UvrD had to be activated by MutSL (Supplementary Figure S10). Taken together, these results indicate that removal of the daughter strand by UvrD and exonuclease is significantly more ef-

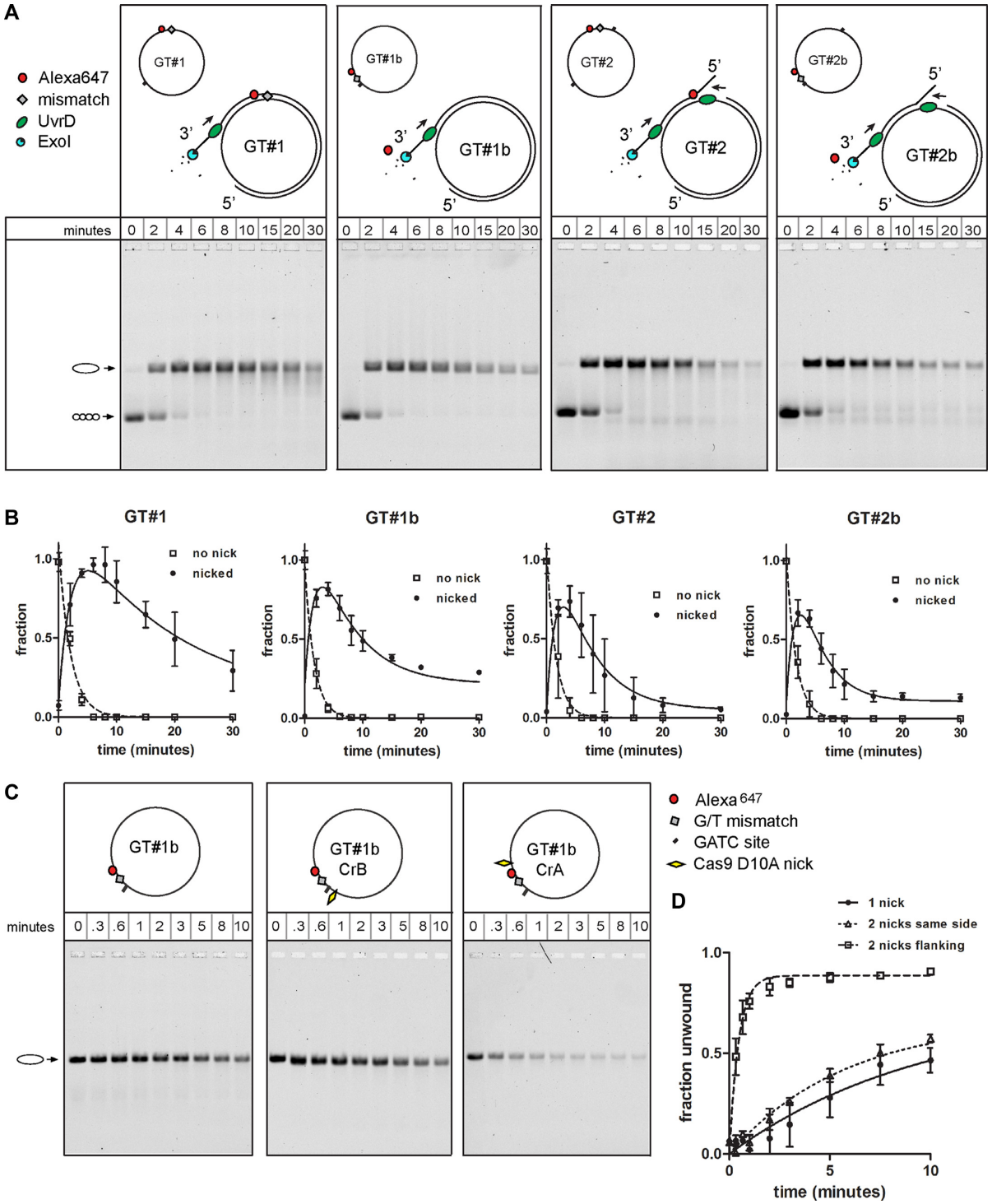

Figure 6. Acceleration of daughter strand unwinding and degradation by GATC sites flanking the mismatch. (**A**) Agarose gel analysis of nicking and unwinding of 0.5 nM circular DNA containing a single G/T mismatch at different positions and one or two GATC sites by 10 nM MutS, 10 nM MutL, 5 nM MutH, 5 nM UvrD, 200 nM Ssb and 0.1 units of ExoI. Early time points (2 and 4 min) showed the conversion of the closed circular DNA (lower band) to open-circular DNA (upper band) due to nicking by MutH. Later time points showed unwinding of nicked daughter strand by UvrD and degradation by ExoI starting from the 3′ end as indicated in the schematic drawings above the gel panels. (**B**) Quantification of the fraction of unnicked and nicked DNA for GT#1, GT#1b, GT#2 and GT#2b (mean ± SD, n = 3) with fit according to the unwinding model. Kinetic parameters obtained from the fit are tabulated in Supplementary Table S4. (**C**) Unwinding and excision of GT#1b pre-nicked with MutH alone (left panel), with MutH and Cas9 at site CrB such that nicks were on the same side of the mismatch (middle panel), and with MutH and Cas9 at site CrA such that the nicks flank the mismatch (right panel). (**D**) Quantification of unwinding (mean ± SD, n = 3) and fit with a function describing a single exponential increase. Kinetic parameters obtained from the fits are tabulated in Supplementary Table S4.

ficient when two nicks are flanking the mismatch in close proximity.

Multiple nicks facilitate human mismatch repair

We assessed whether multiple nicks can also be utilized in human MMR. In eukaryotes, a MutH homologue is not present, but the latent endonuclease activity resides in MutLα (25), which is required for repair of substrates with a pre-existing nick residing 3′ from the mismatch (9,25,58). If a single nick is located 5′ from the mismatch, MutLα is not essential for repair in a system reconstituted from purified human proteins (58), or in human nuclear extracts (59). Using nuclear extracts of HEK293T cells that lack MutLα (51), we tested whether multiple nicks created by MutLα are used for repair, even when a single 5′ nick is available. Repair of a G/T mismatch was scored on circular substrates with a nick 184 bp 3′ from the mismatch, 363 bp 5′ from the mismatch, or both, through restoration of an AclI restriction site. As expected, the G/T mismatch was not repaired in the absence of MutLα when only a single 3′ nick was available (Figure 7A and D). Supplementing the 293T nuclear extracts with purified recombinant MutLα restored repair (Figure 7C and F), while the nuclease-deficient MLH1/PMS2-D699N (MutLα-DN) variant failed to do so (Figure 7B and E). When a 5′ nick was present, a considerable amount of repair occurred in the absence of MutLα (Figure 7A and D). This repair efficiency increased slightly when MutLα was present (Figure 7C and F), similar to results obtained with MutLα-depleted or -deficient extracts (60). However, MutLα-DN was unable to increase the efficiency of repair (Figure 7B and E). The presence of both 5′ and 3′ nicks in the human system further increased repair efficiencies compared to only a single 5′ nick. Collectively, our results indicate that, also during human MMR, multiple nicks are used for repair.

DISCUSSION

GATC site distribution does not influence the efficiency of strand incision

During DNA mismatch repair, strand discrimination is the crucial step that determines whether a detected replication error will be correctly repaired or not. In all organisms, the signal that allows discrimination is transient, providing MMR with a limited window of opportunity to initiate repair. Here, we showed for *E. coli* MMR that, for distances of up to 1 kb, MutS, MutL and MutH were able to efficiently nick GATC sites, irrespective of the distance between the mismatch and this GATC site and largely independent of the number of GATC sites (Figure 1). Thus, within the context of the complete incision reaction, communication between the mismatch and the GATC site occurred rapidly. We note that the purpose of the experiments described here was not to explicitly address the *mode* of communication between mismatch and GATC site. However, according to the diffusion coefficient of the MutS sliding clamp [0.1 $\mu m^2 s^{-1}$ at 150 mM NaCl as estimated from Figure 2B in (61)] MutS is able to move over more than 1 kb of the DNA within one second. Thus, if diffusion indeed occurs within the context of the incision complex, its relative contribution to the overall nicking rate will be small.

Taken together, our results imply (1) that the rate-limiting step during strand discrimination is the formation of an active incision complex, rather than communication between the mismatch and the GATC site, and (2) the effect of GATC site distribution on *in vivo* and *in vitro* repair efficiencies (4,39,40) is most likely not caused by differences in the rate of daughter strand incision, but will be dominated by downstream reaction steps such as DNA strand unwinding and excision. This is supported by recent *in vivo* data indicating that the GATC site distribution influences repair efficiency through determining excision tract length rather than through influencing the efficiency of strand incision (42).

The MMR incision complex acts processively to create multiple daughter strand nicks

When two GATC sites were present on a mismatched DNA substrate, both sites were nicked rapidly (Figure 2). We used a simple mathematical model combining two successive first-order reactions to analyze our data. The first reaction (with rate constant k_1) described the disappearance of the closed circular substrate, which encapsulates complex formation of the MMR protein(s) with DNA and the incision of one of the GATC sites as a single enzymatic step. The second reaction describes the conversion of the intermediate with a single nick into product in which both sites are nicked (with a rate constant k_2). When data obtained from mismatch-independent incision by MutH were fitted with this model, we found that k_1 was approximately three times faster than k_2. However, during mismatch-dependent incision in the presence of MutS, MutL and MutH, k_2 was faster than k_1, even under conditions that inhibited multiple loading of MutS (Figure 3). This indicates that the two incisions were introduced in a processive manner because they shared a rate-limiting step. This finding does not mean that multiple loading cannot occur under physiological conditions, but it does underscore the processive capability of the MMR incision complex.

The rate constant for the first incision (k_1) was obtained from fitting the data with a single exponential decay, which assume one discreet enzymatic step. Because incision requires the successive binding and activation of three proteins on the DNA, this model will not be correct for timescales at which these proteins assemble. Indeed under some conditions a lag phase was clearly present before the first incision takes place (Figure 1D). This lag phase is composed of steps such as mismatch detection by MutS, recruitment of MutL by activated MutS, recruitment of MutH by activated MutL (or activation of MutH pre-bound at a GATC site) and ATP-induced conformational changes that may become rate-limiting at high protein concentrations allowing rapid protein recruitment (55,62). A more complex model as well as additional data would be required to more accurately assess these events, but our data suggest that assembly and activation of the incision complex would occur between 5 and 30 s. This is in agreement with the reported lifetimes of several seconds for intermediate MutS

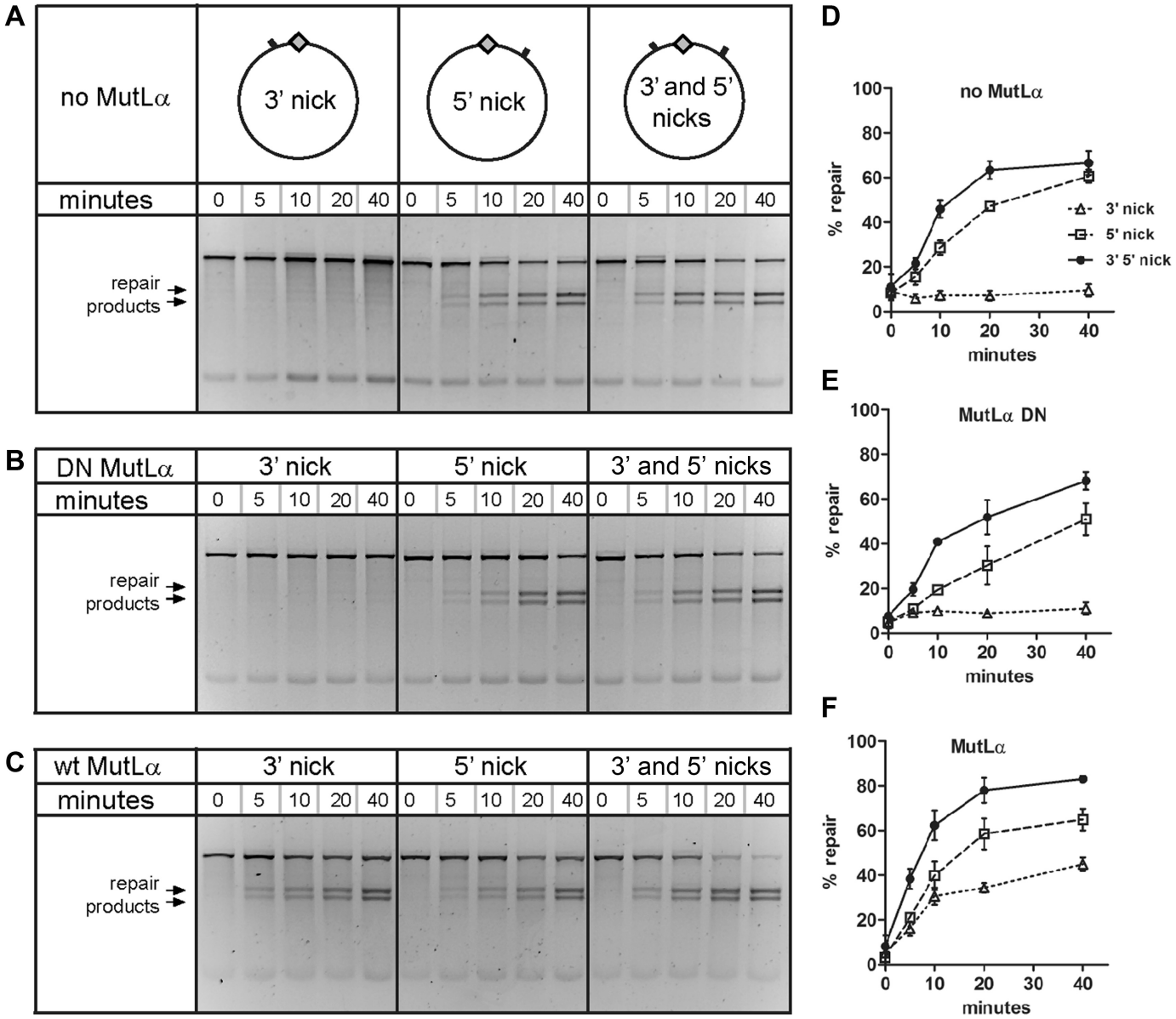

Figure 7. Multiple nicks are beneficial for mismatch repair in human nuclear extracts. Substrates carrying a single G/T mismatch and a single pre-existing nick 363 bp 5′ form the mismatch, a single pre-existing nick 184 bp 3' from the mismatch, or both 5′ and 3′ nicks, were incubated with HEK293T nuclear extracts. Repair of the G/T mismatch was scored as restoration of an AclI restriction site. (**A**) HEK293T nuclear extracts lacking MutLα repaired a G/T mismatch only when a 5' nick was present. (**B**) Supplementing the extracts with MutLα-DN, which is deficient in endonuclease activity, did not restore repair of the 3′ nicked substrate, nor did it enhance repair of the 5′ nicked substrate. (**C**) Addition of wild type MutLα restored repair on the 3′ substrate, and increased MMR efficiency on the 5′ substrate and the substrate with 2 flanking nicks. (**D**–**F**). Panels on the right contain data points with error bars representing means ± SEM of three independent experiments.

states and the duration of slow conformational changes in MutS and MutL (55,61–64).

The processive capability could be determined from experiments in which multiple loading was minimized. At stoichiometric protein and DNA concentrations k_2 was up to 7-fold higher than k_1 (Figure 4C; Supplementary Table S1), indicating that a major fraction of the nicking events was processive. Under single-turnover conditions, created upon addition of a DNA trap, 86% of the DNA substrate that was prebound by MutS was incised twice (Figure 3D). Processive behavior was furthermore supported by the differential contributions of MutS, MutL and MutH to k_1 and k_2. When MutS concentration was varied while MutL and MutH remained constant, under conditions where multiple loading was unlikely, we observed that k_1 increased with the MutS concentration, but k_2 did not, which was reflected in the k_2/k_1 ratio (Figure 4A–C). The higher MutS concentration increased the rate of formation of the mismatch recognition complex, which is a necessary intermediate in the first incision event. However, the concentration-independence of k_2 indicated that MutS does not have to be loaded again for the second incision, in agreement with the results from

the single turnover experiment with the DNA trap. When MutL or MutH were titrated, both k_1 and k_2 were affected, but in a similar manner. This is also reflected in the k_2/k_1 ratio. We therefore conclude that both MutL and MutH were recruited anew for the second nicking event, and that a single MutS sliding clamp was able to repeatedly load MutL. Multiple loading of MutL is supported by *in vitro* single molecule studies (63) and *in vivo* fluorescence analysis (65,66).

At high MutS concentrations (500 nM) allowing rapid multiple loading, an interesting difference between MutL and MutH became apparent. Decreasing the MutL concentration strongly reduced the processive character of the reaction, while decreasing MutH did not (Figure 4D). Apparently, even at low concentrations MutH was able to efficiently sample multiple pre-incision complexes present on the DNA at high concentrations of MutS and MutL, indicating that the interaction between the endonuclease and activated MutL is dynamic. In contrast, the small amount of MutL that was properly recruited to activate the first incision event was unable to induce the second incision, suggesting that MutL was unable to rapidly sample multiple MutS sliding clamps. Furthermore, our analysis of MutL variant K307A suggested that the nucleotide-bound, closed form of MutL is required for efficient and processive incision and that processivity is influenced by MutH (Figure 5), in agreement with the observations that MutH induces ATP binding in MutL (16). Also taking into consideration that MutL modulates the sliding behavior of MutS (48,63,67,68), and may unload sliding clamps (16), these observations indicate that the action of MutL is complex and requires further detailed analysis. We have summarized our findings in an incision model, in which a single MutS binding event enables processive nicking of GATC sites through recruiting and activating multiple MutL and MutH molecules (Figure 8A).

GATC sites flanking the mismatch increase the efficiency of daughter strand unwinding and removal in *E. coli* MMR

Because on our substrates the fluorophore is located in close proximity to the mismatch (14 and 15 bp on GT#2 and GT#2b, respectively), the disappearance of the fluorescent signal is a measure for mismatch removal. At identical reaction conditions with equimolar concentrations of the MMR proteins, the observed mismatch removal rate from GT#2 (0.084 ± 0.01 nM DNA/min) was approximately 4-fold slower than the nicking rate (0.31 ± 0.03 nM DNA/min for the first incision). This is in agreement with previous observations that nicked circles are produced fast enough to accumulate as reaction intermediates (53) and supports the idea that increasing the distance between the mismatch and the GATC site may reduce repair efficiency because of steps downstream from nicking. We found an approximate 3-fold enhancement of the unwinding and excision rates upon decreasing the distance between the mismatch and the GATC site from 1042 to 61 bp on GT#1 (Figure 6A and B), in agreement with *in vivo* repair efficiencies being determined by the length of excision tracts (42).

The rate for mismatch removal from a substrate with two GATC sites flanking the mismatch was faster than for substrates with a single site, or two sites situated on the same side of the mismatch. This was observed on substrates with one site close to and one site far from the mismatch, and more prominent on substrates with both pre-existing nicks in close proximity to the mismatch (Figure 6). An intuitive explanation for the increase in efficiency on the substrates with one site close and one site far away from the mismatch involves loading of UvrD on both flanking GATC sites, resulting in convergent unwinding from two sites, which would effectively double the unwinding rate. This explanation might appear unlikely, as ExoI can only degrade ssDNA from the 3′ end. However, it becomes plausible when one takes into account the likely displacement of the double-nicked fragment from the DNA substrate, which would make it readily available for degradation by ExoI, as compared to the singly-nicked substrate in which the unwound terminus can reanneal to the template strand and thus hinder its degradation. This hypothesis is supported by the unwinding reactions carried out in the absence of ExoI, in which the displaced strand from GT#15 was visible as a reaction intermediate, while unwinding of GT#1 and GT#1b resulted in the formation of high-molecular weight species that might have arisen through inter-molecular annealing of the displaced daughter strands (Supplementary Figure S9). This is also in agreement with the substantial increase (13-fold) in the unwinding and excision rate when the mismatch is flanked by two nicks in close proximity (Figure 6C and D); the relatively short DNA fragment spanning the mismatch could be completely removed by a single UvrD unwinding event.

Combining our findings from nicking and unwinding kinetics on substrates with two GATC sites, we observe that MMR complexes processively introduce multiple daughter strand nicks, thereby circumventing the slow reassembly of active incision complexes for each subsequent nicking event. Not only does this ensure increased availability of strand discrimination signals before GATC sites become inaccessible to nicking through Dam methylation, but flanking nicks also increase the rate of daughter strand unwinding, thereby increasing overall repair efficiencies (Figure 8B).

Multiple strand incisions increase the efficiency of human MMR

In contrast to *E. coli* and a number of additional Gram-negative bacteria, most organisms lack MutH (69). Instead, these organisms contain a latent endonuclease activity residing in the MutL homodimer, respectively, in the PMS subunit of the MutLα heterodimer (25,31,34). MutLα is not essential for MMR on substrates containing a pre-existing 5′ nick, because MutSα is able to activate EXO1, a 5′ to 3′ exonuclease, to catalyze a limited degradation of the error-containing strand (8,70). Nevertheless, in nuclear extracts of human cells, the presence of MutLα not only allows repair of substrates with a 3′ pre-existing nick, but also results in an increased repair efficiency of substrates with a pre-existing 5′- nick (60,70,71). We only observed this increased efficiency in our *in vitro* MMR assay upon addition of nuclease-proficient MutLα and not with the nuclease-deficient variant (Figure 7). This implies that, as we ob-

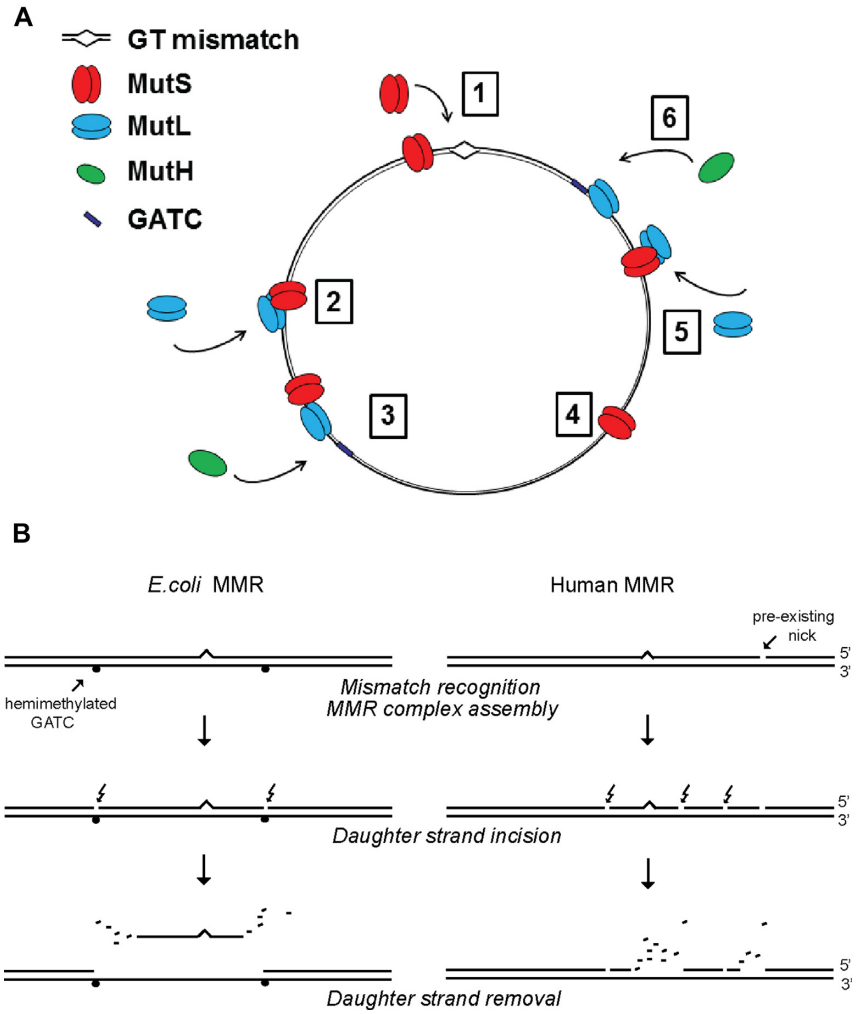

Figure 8. Models of processive daughter strand incision showing how its functional conservation contributes to efficient DNA excision during mismatch repair in bacteria and eukaryotes. (**A**) Model for processive nicking during *E.coli* MMR. MutS binds the mismatch and forms a sliding clamp (1). The sliding clamp recruits MutL (2), which needs to change conformation from an open state into a closed state to activate MutH to incise the DNA at the GATC site (3). The same activated MutS (4) then loads an additional MutL (5) which can initiate the second incision upon activating a new molecule of MutH (6). If MutS sliding is diffusive, MutS either continues sliding in the same direction after the first incision, approaching the second GATC site along the long path (as indicated here); or (at any moment) reverses direction, passing over the mismatch (for which it is blind as long as it contains ATP in both subunits) and approaching the second GATC along the short path. (**B**) Functional conservation of multiple daughter strand incision. On the left: The schematic steps of MMR in *E. coli* and other Gram-negative bacteria that rely on the incision of hemi-methylated GATC sites by the MutH endonuclease for strand discrimination. Mismatch detection results in the assembly of an incision complex that is able to introduce multiple nicks into the daughter strand at hemi-methylated GATC sites in the vicinity of the mismatch. This allows unwinding and excision to start simultaneously from both ends of the DNA fragment flanking the mismatch. On the right: the schematic steps of MMR in organisms that rely on the endonuclease activity of MutL or MutLα to introduce nicks into the daughter strand. This endonuclease is activated in a directional manner by the β-clamp or PCNA that is loaded at a pre-existing nick, and creates multiple daughter strand nicks in the vicinity of the mismatch. The resulting small DNA fragment containing the mismatch can then be rapidly removed by exonucleases or displaced by a polymerase.

served for *E. coli*, mammalian MMR also benefits from the introduction of multiple nicks in the vicinity of the mismatch.

Substrates containing two pre-existing flanking nicks in the vicinity of the mismatch were corrected with higher efficiency than substrates with a single pre-existing nick, both in the absence and presence of functional MutLα (Figure 7). The eukaryotic system does not have a helicase that can displace the double-nicked strand. Degradation is dependent solely on the activity of EXO1, or on the strand displacement activity of polymerase-δ, both of which have an obligate 5′ to 3′ polarity. We speculate that the pre-existing nicks flanking the mismatch define the length of the excision tract and increase the efficiency of strand removal, even when additional nicks will be rapidly introduced in close proximity of the mismatch once the mismatch-activated MutSα/MutLα complex interacts with PCNA loaded at a nick (32,36).

Evolutionary implications

In all organisms, the rapid introduction of nicks into an error-containing newly-synthesized strand ensures that MMR can efficiently remove the misincorporated nu-

cleotide(s) within the brief time window during which discrimination between the template and the daughter strand is possible. Generation of multiple nicks may be a safety mechanism that reduces the likelihood of disappearance of the strand discrimination signal due to nick ligation. In addition, it may increase the rates of unwinding, excision and repair (Figure 8B). This may be particularly important *in vivo* if MMR predominantly relies on the MutS or MutSα that is traveling with the replication fork (42) rather than on multiple loading. This indicates that, despite significant mechanistic differences in strand discrimination between different organisms, the common feature of MMR that is conserved in evolution is the introduction of multiple nicks in the vicinity of the misincorporated nucleotide, which enhance the efficiency of daughter strand removal and repair.

SUPPLEMENTARY DATA

Supplementary Data are available at NAR Online.

ACKNOWLEDGEMENTS

We are grateful to Wei Yang for the pET11d-UvrD expression construct, to Farid A. Kadyrov for the expression vector for the MLH1/PMS2-D699N variant, and to Kalpana Surendranath and Anja Saxer for purification of MutLα proteins.

FUNDING

European Community's Seventh Framework Programme (FP7/2007-2013) under grant agreement nº HEALTH-F4-2008-223545; by a VIDI grant [700.58.428 to J.L.] and Gravitation program 'Cancer Genomics Netherlands' from the Netherlands Organization for Scientific Research (NWO); ERC grant 'MIRIAM' [294537 to J.J., M.A.-B]. Funding for open access charge: Netherlands Organization for Scientific Research (NWO).
Conflict of interest statement. None declared.

REFERENCES

1. Kunkel,T.A. and Erie,D.A. (2015) Eukaryotic mismatch repair in relation to DNA replication. *Annu. Rev. Genet.*, **49**, 291–313.
2. Jiricny,J. (2013) Postreplicative mismatch repair. *Cold Spring Harb. Perspect. Biol.*, **5**, a012633.
3. Lahue,R.S., Au,K.G. and Modrich,P. (1989) DNA mismatch correction in a defined system. *Science*, **245**, 160–164.
4. Lahue,R.S., Su,S.S. and Modrich,P. (1987) Requirement for d(GATC) sequences in Escherichia coli mutHLS mismatch correction. *Proc. Natl. Acad. Sci. U.S.A.*, **84**, 1482–1486.
5. Dao,V. and Modrich,P. (1998) Mismatch-, MutS-, MutL-, and helicase II-dependent unwinding from the single-strand break of an incised heteroduplex. *J. Biol. Chem.*, **273**, 9202–9207.
6. Viswanathan,M., Burdett,V., Baitinger,C., Modrich,P. and Lovett,S.T. (2001) Redundant exonuclease involvement in Escherichia coli methyl-directed mismatch repair. *J. Biol. Chem.*, **276**, 31053–31058.
7. Tishkoff,D.X., Amin,N.S., Viars,C.S., Arden,K.C. and Kolodner,R.D. (1998) Identification of a human gene encoding a homologue of Saccharomyces cerevisiae EXO1, an exonuclease implicated in mismatch repair and recombination. *Cancer Res.*, **58**, 5027–5031.
8. Genschel,J., Bazemore,L.R. and Modrich,P. (2002) Human exonuclease I is required for 5' and 3' mismatch repair. *J. Biol. Chem.*, **277**, 13302–13311.
9. Kadyrov,F.A., Genschel,J., Fang,Y., Penland,E., Edelmann,W. and Modrich,P. (2009) A possible mechanism for exonuclease 1-independent eukaryotic mismatch repair. *Proc. Natl. Acad. Sci. U.S.A.*, **106**, 8495–8500.
10. Su,S.S. and Modrich,P. (1986) Escherichia coli mutS-encoded protein binds to mismatched DNA base pairs. *Proc. Natl. Acad. Sci. U.S.A.*, **83**, 5057–5061.
11. Jiricny,J., Hughes,M., Corman,N. and Rudkin,B.B. (1988) A human 200-kDa protein binds selectively to DNA fragments containing G.T mismatches. *Proc. Natl. Acad. Sci. U.S.A.*, **85**, 8860–8864.
12. Lamers,M.H., Perrakis,A., Enzlin,J.H., Winterwerp,H.H., de Wind,N. and Sixma,T.K. (2000) The crystal structure of DNA mismatch repair protein MutS binding to a G x T mismatch. *Nature*, **407**, 711–717.
13. Warren,J.J., Pohlhaus,T.J., Changela,A., Iyer,R.R., Modrich,P.L. and Beese,L.S. (2007) Structure of the human MutSalpha DNA lesion recognition complex. *Mol. Cell*, **26**, 579–592.
14. Groothuizen,F.S. and Sixma,T.K. (2016) The conserved molecular machinery in DNA mismatch repair enzyme structures. *DNA Repair (Amst)*, **38**, 14–23.
15. Gradia,S., Acharya,S. and Fishel,R. (1997) The human mismatch recognition complex hMSH2-hMSH6 functions as a novel molecular switch. *Cell*, **91**, 995–1005.
16. Acharya,S., Foster,P.L., Brooks,P. and Fishel,R. (2003) The coordinated functions of the E. coli MutS and MutL proteins in mismatch repair. *Mol. Cell*, **12**, 233–246.
17. Lebbink,J.H., Georgijevic,D., Natrajan,G., Fish,A., Winterwerp,H.H., Sixma,T.K. and de Wind,N. (2006) Dual role of MutS glutamate 38 in DNA mismatch discrimination and in the authorization of repair. *EMBO J.*, **25**, 409–419.
18. Gradia,S., Subramanian,D., Wilson,T., Acharya,S., Makhov,A., Griffith,J. and Fishel,R. (1999) hMSH2-hMSH6 forms a hydrolysis-independent sliding clamp on mismatched DNA. *Mol. Cell*, **3**, 255–261.
19. Grilley,M., Welsh,K.M., Su,S.S. and Modrich,P. (1989) Isolation and characterization of the Escherichia coli mutL gene product. *J. Biol. Chem.*, **264**, 1000–1004.
20. Blackwell,L.J., Wang,S. and Modrich,P. (2001) DNA chain length dependence of formation and dynamics of hMutSalpha.hMutLalpha.heteroduplex complexes. *J. Biol. Chem.*, **276**, 33233–33240.
21. Raschle,M., Dufner,P., Marra,G. and Jiricny,J. (2002) Mutations within the hMLH1 and hPMS2 subunits of the human MutLalpha mismatch repair factor affect its ATPase activity, but not its ability to interact with hMutSalpha. *J. Biol. Chem.*, **277**, 21810–21820.
22. Friedhoff,P., Li,P. and Gotthardt,J. (2016) Protein-protein interactions in DNA mismatch repair. *DNA Repair (Amst)*, **38**, 50–57.
23. Junop,M.S., Yang,W., Funchain,P., Clendenin,W. and Miller,J.H. (2003) In vitro and in vivo studies of MutS, MutL and MutH mutants: correlation of mismatch repair and DNA recombination. *DNA Repair (Amst)*, **2**, 387–405.
24. Mechanic,L.E., Frankel,B.A. and Matson,S.W. (2000) Escherichia coli MutL loads DNA helicase II onto DNA. *J. Biol. Chem.*, **275**, 38337–38346.
25. Kadyrov,F.A., Dzantiev,L., Constantin,N. and Modrich,P. (2006) Endonucleolytic function of MutLalpha in human mismatch repair. *Cell*, **126**, 297–308.
26. Langle-Rouault,F., Maenhaut-Michel,G. and Radman,M. (1987) GATC sequences, DNA nicks and the MutH function in Escherichia coli mismatch repair. *EMBO J.*, **6**, 1121–1127.
27. Barras,F. and Marinus,M.G. (1989) The great GATC: DNA methylation in E. coli. *Trends Genet.*, **5**, 139–143.
28. Campbell,J.L. and Kleckner,N. (1990) E. coli oriC and the dnaA gene promoter are sequestered from dam methyltransferase following the passage of the chromosomal replication fork. *Cell*, **62**, 967–979.
29. Welsh,K.M., Lu,A.L., Clark,S. and Modrich,P. (1987) Isolation and characterization of the Escherichia coli mutH gene product. *J. Biol. Chem.*, **262**, 15624–15629.
30. Putnam,C.D. (2016) Evolution of the methyl directed mismatch repair system in Escherichia coli. *DNA Repair (Amst)*, **38**, 32–41.
31. Pillon,M.C., Lorenowicz,J.J., Uckelmann,M., Klocko,A.D., Mitchell,R.R., Chung,Y.S., Modrich,P., Walker,G.C., Simmons,L.A.,

Friedhoff,P. *et al.* (2010) Structure of the endonuclease domain of MutL: unlicensed to cut. *Mol. Cell*, **39**, 145–151.
32. Pluciennik,A., Dzantiev,L., Iyer,R.R., Constantin,N., Kadyrov,F.A. and Modrich,P. (2010) PCNA function in the activation and strand direction of MutLalpha endonuclease in mismatch repair. *Proc. Natl. Acad. Sci. U.S.A.*, **107**, 16066–16071.
33. Guarne,A. (2012) The functions of MutL in mismatch repair: the power of multitasking. *Prog. Mol. Biol. Transl. Sci.*, **110**, 41–70.
34. Kadyrov,F.A., Holmes,S.F., Arana,M.E., Lukianova,O.A., O'Donnell,M., Kunkel,T.A. and Modrich,P. (2007) Saccharomyces cerevisiae MutLalpha is a mismatch repair endonuclease. *J. Biol. Chem.*, **282**, 37181–37190.
35. Goellner,E.M., Smith,C.E., Campbell,C.S., Hombauer,H., Desai,A., Putnam,C.D. and Kolodner,R.D. (2014) PCNA and Msh2-Msh6 activate an Mlh1-Pms1 endonuclease pathway required for Exo1-independent mismatch repair. *Mol. Cell*, **55**, 291–304.
36. Pena-Diaz,J. and Jiricny,J. (2010) PCNA and MutLalpha: partners in crime in triplet repeat expansion? *Proc. Natl. Acad. Sci. U.S.A.*, **107**, 16409–16410.
37. Ghodgaonkar,M.M., Lazzaro,F., Olivera-Pimentel,M., Artola-Boran,M., Cejka,P., Reijns,M.A., Jackson,A.P., Plevani,P., Muzi-Falconi,M. and Jiricny,J. (2013) Ribonucleotides misincorporated into DNA act as strand-discrimination signals in eukaryotic mismatch repair. *Mol. Cell*, **50**, 323–332.
38. Lujan,S.A., Williams,J.S., Clausen,A.R., Clark,A.B. and Kunkel,T.A. (2013) Ribonucleotides are signals for mismatch repair of leading-strand replication errors. *Mol. Cell*, **50**, 437–443.
39. Lu,A.L. (1987) Influence of GATC sequences on Escherichia coli DNA mismatch repair in vitro. *J. Bacteriol.*, **169**, 1254–1259.
40. Bruni,R., Martin,D. and Jiricny,J. (1988) d(GATC) sequences influence Escherichia coli mismatch repair in a distance-dependent manner from positions both upstream and downstream of the mismatch. *Nucleic Acids Res.*, **16**, 4875–4890.
41. Lahue,R.S. and Modrich,P. (1988) Methyl-directed DNA mismatch repair in Escherichia coli. *Mutat Res.*, **198**, 37–43.
42. Hasan,A.M. and Leach,D.R. (2015) Chromosomal directionality of DNA mismatch repair in Escherichia coli. *Proc. Natl. Acad. Sci. U.S.A.*, **112**, 9388–9393.
43. Cooper,D.L., Lahue,R.S. and Modrich,P. (1993) Methyl-directed mismatch repair is bidirectional. *J. Biol. Chem.*, **268**, 11823–11829.
44. Natrajan,G., Lamers,M.H., Enzlin,J.H., Winterwerp,H.H., Perrakis,A. and Sixma,T.K. (2003) Structures of Escherichia coli DNA mismatch repair enzyme MutS in complex with different mismatches: a common recognition mode for diverse substrates. *Nucleic Acids Res.*, **31**, 4814–4821.
45. Guarne,A., Ramon-Maiques,S., Wolff,E.M., Ghirlando,R., Hu,X., Miller,J.H. and Yang,W. (2004) Structure of the MutL C-terminal domain: a model of intact MutL and its roles in mismatch repair. *EMBO J.*, **23**, 4134–4145.
46. Lebbink,J.H., Fish,A., Reumer,A., Natrajan,G., Winterwerp,H.H. and Sixma,T.K. (2010) Magnesium coordination controls the molecular switch function of DNA mismatch repair protein MutS. *J. Biol. Chem.*, **285**, 13131–13141.
47. Tham,K.C., Hermans,N., Winterwerp,H.H., Cox,M.M., Wyman,C., Kanaar,R. and Lebbink,J.H. (2013) Mismatch repair inhibits homeologous recombination via coordinated directional unwinding of trapped DNA structures. *Mol. Cell*, **51**, 326–337.
48. Groothuizen,F.S., Winkler,I., Cristovao,M., Fish,A., Winterwerp,H.H., Reumer,A., Marx,A.D., Hermans,N., Nicholls,R.A., Murshudov,G.N. *et al.* (2015) MutS/MutL crystal structure reveals that the MutS sliding clamp loads MutL onto DNA. *Elife*, **4**, e06744.
49. Feng,G. and Winkler,M.E. (1995) Single-step purifications of His6-MutH, His6-MutL and His6-MutS repair proteins of escherichia coli K-12. *Biotechniques*, **19**, 956–965.
50. Runyon,G.T. and Lohman,T.M. (1989) Escherichia coli helicase II (uvrD) protein can completely unwind fully duplex linear and nicked circular DNA. *J. Biol. Chem.*, **264**, 17502–17512.
51. Baerenfaller,K., Fischer,F. and Jiricny,J. (2006) Characterization of the 'mismatch repairosome' and its role in the processing of modified nucleosides in vitro. *Methods Enzymol.*, **408**, 285–303.
52. Hegedus,E., Kokai,E., Kotlyar,A., Dombradi,V. and Szabo,G. (2009) Separation of 1-23-kb complementary DNA strands by urea-agarose gel electrophoresis. *Nucleic Acids Res.*, **37**, e112.
53. Au,K.G., Welsh,K. and Modrich,P. (1992) Initiation of methyl-directed mismatch repair. *J. Biol. Chem.*, **267**, 12142–12148.
54. Feng,G., Tsui,H.C. and Winkler,M.E. (1996) Depletion of the cellular amounts of the MutS and MutH methyl-directed mismatch repair proteins in stationary-phase Escherichia coli K-12 cells. *J. Bacteriol.*, **178**, 2388–2396.
55. Qiu,R., DeRocco,V.C., Harris,C., Sharma,A., Hingorani,M.M., Erie,D.A. and Weninger,K.R. (2012) Large conformational changes in MutS during DNA scanning, mismatch recognition and repair signalling. *EMBO J.*, **31**, 2528–2540.
56. Ban,C., Junop,M. and Yang,W. (1999) Transformation of MutL by ATP binding and hydrolysis: a switch in DNA mismatch repair. *Cell*, **97**, 85–97.
57. Grilley,M., Griffith,J. and Modrich,P. (1993) Bidirectional excision in methyl-directed mismatch repair. *J. Biol. Chem.*, **268**, 11830–11837.
58. Zhang,Y., Yuan,F., Presnell,S.R., Tian,K., Gao,Y., Tomkinson,A.E., Gu,L. and Li,G.M. (2005) Reconstitution of 5'-directed human mismatch repair in a purified system. *Cell*, **122**, 693–705.
59. Constantin,N., Dzantiev,L., Kadyrov,F.A. and Modrich,P. (2005) Human mismatch repair: reconstitution of a nick-directed bidirectional reaction. *J. Biol. Chem.*, **280**, 39752–39761.
60. Genschel,J. and Modrich,P. (2009) Functions of MutLalpha, replication protein A (RPA), and HMGB1 in 5'-directed mismatch repair. *J. Biol. Chem.*, **284**, 21536–21544.
61. Cho,W.K., Jeong,C., Kim,D., Chang,M., Song,K.M., Hanne,J., Ban,C., Fishel,R. and Lee,J.B. (2012) ATP alters the diffusion mechanics of MutS on mismatched DNA. *Structure*, **20**, 1264–1274.
62. Sharma,A., Doucette,C., Biro,F.N. and Hingorani,M.M. (2013) Slow conformational changes in MutS and DNA direct ordered transitions between mismatch search, recognition and signaling of DNA repair. *J. Mol. Biol.*, **425**, 4192–4205.
63. Qiu,R., Sakato,M., Sacho,E.J., Wilkins,H., Zhang,X., Modrich,P., Hingorani,M.M., Erie,D.A. and Weninger,K.R. (2015) MutL traps MutS at a DNA mismatch. *Proc. Natl. Acad. Sci. U.S.A.*, **112**, 10914–10919.
64. Jeong,C., Cho,W.K., Song,K.M., Cook,C., Yoon,T.Y., Ban,C., Fishel,R. and Lee,J.B. (2011) MutS switches between two fundamentally distinct clamps during mismatch repair. *Nat. Struct. Mol. Biol.*, **18**, 379–385.
65. Elez,M., Radman,M. and Matic,I. (2012) Stoichiometry of MutS and MutL at unrepaired mismatches in vivo suggests a mechanism of repair. *Nucleic Acids Res.*, **40**, 3929–3938.
66. Hombauer,H., Campbell,C.S., Smith,C.E., Desai,A. and Kolodner,R.D. (2011) Visualization of eukaryotic DNA mismatch repair reveals distinct recognition and repair intermediates. *Cell*, **147**, 1040–1053.
67. Drotschmann,K., Aronshtam,A., Fritz,H.J. and Marinus,M.G. (1998) The Escherichia coli MutL protein stimulates binding of Vsr and MutS to heteroduplex DNA. *Nucleic Acids Res.*, **26**, 948–953.
68. Schofield,M.J., Nayak,S., Scott,T.H., Du,C. and Hsieh,P. (2001) Interaction of Escherichia coli MutS and MutL at a DNA mismatch. *J. Biol. Chem.*, **276**, 28291–28299.
69. Putnam,C.D. (2016) Evolution of the methyl directed mismatch repair system in Escherichia coli. *DNA Repair (Amst)*, **38**, 32–41.
70. Genschel,J. and Modrich,P. (2003) Mechanism of 5'-directed excision in human mismatch repair. *Mol. Cell*, **12**, 1077–1086.
71. Li,G.M. and Modrich,P. (1995) Restoration of mismatch repair to nuclear extracts of H6 colorectal tumor cells by a heterodimer of human MutL homologs. *Proc. Natl. Acad. Sci. U.S.A.*, **92**, 1950–1954.